Abstract

The electrical properties of graphene have proven to be better than many related compounds, such as carbon nanotubes because of its high surface area and electrical conductivity. These properties give graphene potential to enhance electronics, biosensors and potentially battery cells. Scientists are interested in further improving the electrical capabilities of graphene in order to widen its range of application. Wang, Y et al. experimented with n-type doping of graphene in order to intrinsically modify its structure in the hopes of improving its conductivity. Alternatively, Wang, D. et al. used graphene as a structural surface from which to construct a complex of titanium oxide crystals. Both groups used electrochemistry to study the results of their modifications. The outcome of these experiments suggests that graphene is a highly modifiable molecule and has the potential for a wide variety of applications in electrochemistry.

Introduction

The quest for an abundant source of efficient energy is growing evermore important in the modern world. Petroleum supplies are not going to last forever and many in the scientific community are searching for the next major energy source. In interim of the discovery of a new energy source, electronics are becoming more energy efficient in an effort to conserve the remaining energy supply. One way electronic appliances have become more efficient energy consumers is with the advent of lithium ion batteries. Lithium ion batteries are currently used in many portable electronics such as lap top computers, cell phones, and ipods.

Lithium ion batteries owe their popularity to their light weight and high energy storage abilities. Lithium is a highly reactive element because of its single valence electron. The high reactivity of lithium means that a large amount of energy can be stored its chemical bonds[1]. Another popular property of lithium ion batteries is the fact that the battery does not have to be completely dead before recharging it because the chemical reaction going on in the battery is easily reversed when a current is added. The batteries are capable of handling hundreds of charge/discharge cycles, which means they can be drained of power and then reused hundreds of times simply by plugging them in and recharging them.

A lithium ion battery contains a rolled up column of thin sheets that make up the anode and the cathode, as well as one sheet to separate the two electrodes. The cathode is conventionally made of lithium cobalt oxide, and the anode is made of some form of carbon[1]. The middle separation sheet is made of perforated plastic that allows the flow of ions between the electrodes, but doesn't allow them to touch. The column is submerged in an organic solvent such as ether so ions can flow through the cell.

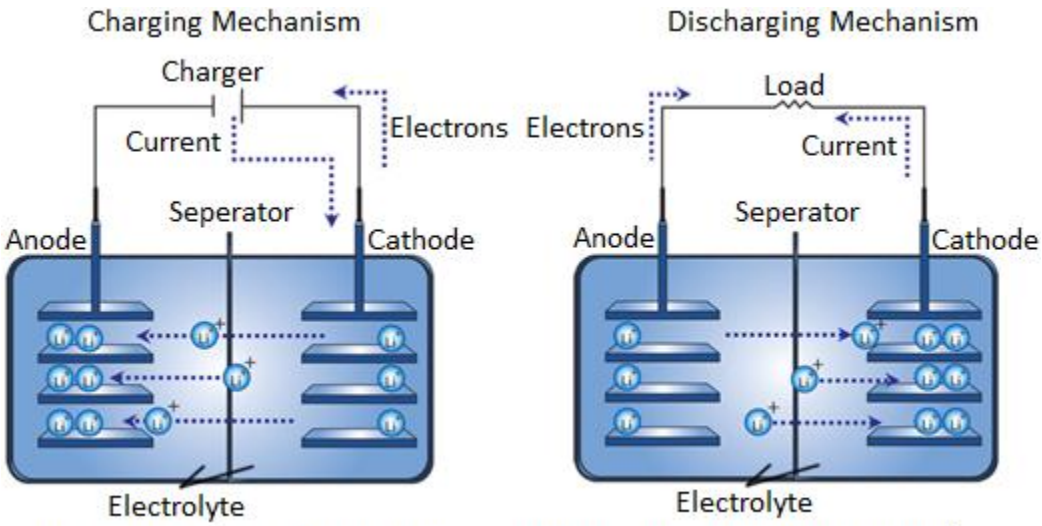

Figure 1. Charge and Discharge mechanisms of a lithium ion battery[1]

When charging, lithium ions are oxidized and move through the cell to bond with the carbon electrode; the anode. The oxidation of lithium proceeds according to the reaction; $Li\ (s) \rightarrow Li^{+} + e^{-}$. When the battery is in use, electrons flow from the anode to the cathode, so lithium ions are reduced and return to the lithium cobalt oxide electrode. The reduction of lithium ions proceeds in the opposite direction; $Li^{+} + e^{-} \rightarrow Li\ (s)$. Figure 1 illustrates how the electrons and lithium ions behave in a cell during charging and discharging. The reduction potential of lithium, E^{0}, is 3.04 volts[2] indicating that this reaction releases a lot of energy, which explains why lithium ion batteries are so powerful. In fact single lithium ion cell produces roughly 3.7 volts[1], or more than twice the typical output of an AA alkaline cell, which is about the same size.

Electrochemical energy storage is a key longevity component of electric vehicles. The batteries of a hybrid or electric vehicle can be up to half the value of the vehicle itself, and right now the batteries last about 10 to 12 years at best.[3] The light weight and high energy density of lithium ion batteries make them attractive for use in electric vehicles, however slow ion diffusion and electron transport[4] limit their effectiveness, and prevent them from widespread use; along with the high cost of battery production. The batteries used in electric vehicles are also subject to high charge/discharge rates, because the battery is constantly switching modes[3]. When the gas pedal is pushed to the floor, the entire voltage of the battery is passed to the engine, and when the pedal is released, no voltage goes to the engine; anything in between requires that the battery be pulsated on an off to achieve the power setting determined by how much the accelerator has been pushed down. For instance, if the accelerator is pushed down half way, the battery has to be turned on half the time and turned off half of the time in order

to supply half of the energy of the battery to the engine. Additionally, to keep the pulsation of the battery that is outside the range of human hearing, the battery must pulsate roughly 15000 times a second[3]. This puts a lot of strain on the battery, and lithium ion batteries do not cope well with this type of strain because they experience increased resistance at the interface of the electrode and the electrolyte at high charge/discharge rates[4]. The stress of high charge and discharging rates decreases the voltage capacity of the batteries, which is an indication of their ability to hold a charge. The voltage capacity of the battery determines how much power can be stored in the cell and therefore determines how useful the battery is.

Despite these flaws, many scientists see a huge advantage to using lithium ion batteries in electric vehicles and other applications should solutions to those problems be attained. Scientists such as Wang, D. *et al*. are searching for ways to resolve the diminishing voltage capacity with increased charge and discharge rates by modifying the electrode materials used in the battery cells.

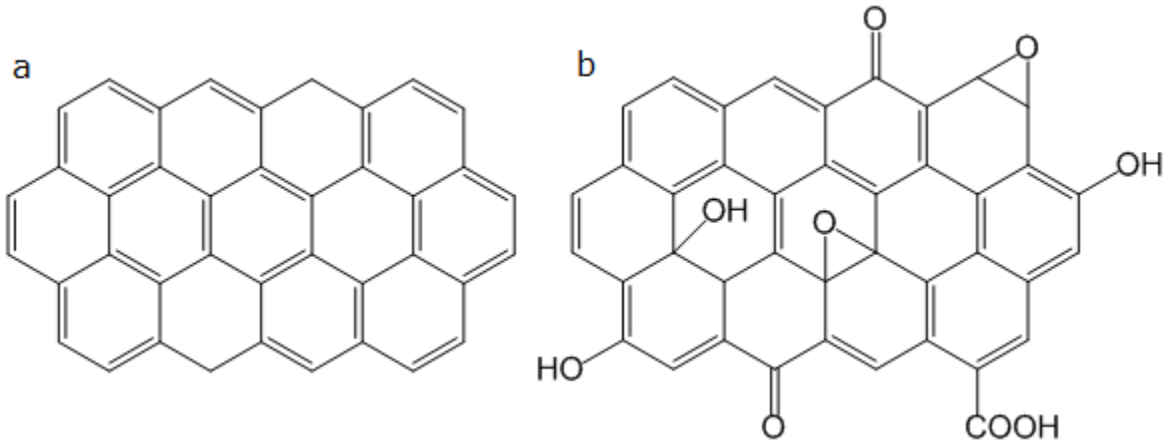

Figure 2. The chemical structure of graphene (a) and graphene oxide (b)

Graphene is a two-dimensional array of sp^2 carbon atoms with a hexagonal lattice structure. Its structure is most easily visualized as chicken wire at the molecular scale. Graphene is a highly conductive species with a high surface area[4-7] which make it ideal for use in electrochemical cells. Graphene is also relatively inexpensive to produce by a variety of methods[4,8,5,6]. Graphene is chemically synthesized in the experiments discussed in this paper by reducing graphene oxide. Graphene oxide is reduced either chemically with hydrazine or by rapid thermal expansion. The structure of graphene and graphene oxide are illustrated in Figures 2a and 2b respectively.

Hydrazine is a common inorganic reducing agent because the byproducts of the reaction are usually nitrogen gas and water[2]. When graphene oxide is reduced by hydrazine, chemically modified graphene is produced[6]. The term chemically modified is used because reduction of graphene oxide with hydrazine does not remove all the impurities in the material and the structural impurities of the parent graphite material are inherited by the graphene product. Carboxyl, carbonyl and hydroxyl groups are not eradicated from the graphene surface strictly by hydrazine reduction as indicated in experiments by Gao *et al*[8]. The mechanisms Gao et al. proposed for the reduction of graphene with hydrazine are presented in Figure 3 below:

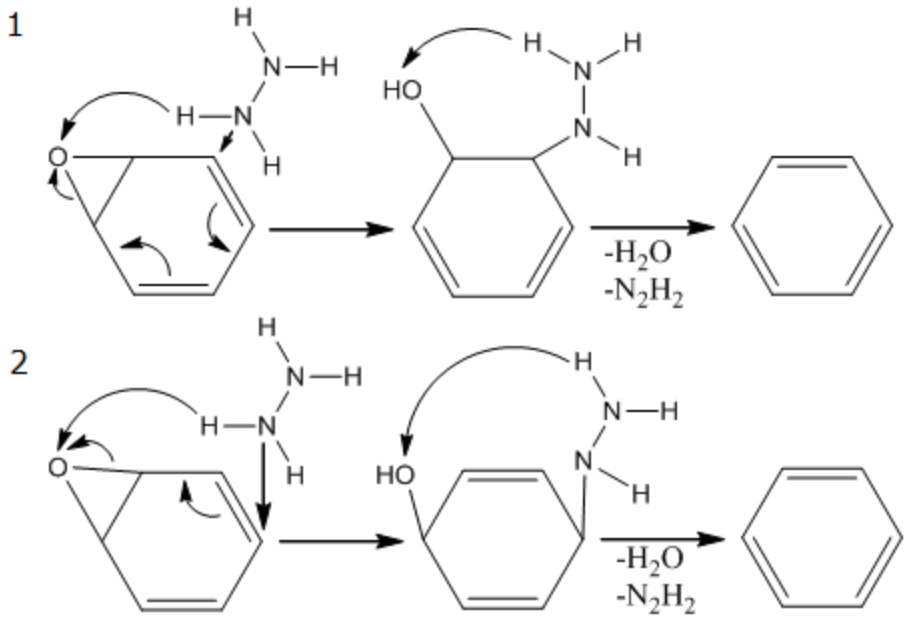

Figure 3. Reaction mechanisms for the chemical reduction of graphene oxide with hydrazine

Reaction mechanisms 1 and 2 are the primary means of de-edpoxidation of graphene oxide with hydrazine according to computational research conducted by Gao *et al*. In mechanism 1, hydrazine attacks the carbon ortho to the epoxide ring and a hydrogen atom is transferred to the oxygen to create a hydrazino alcohol. Then, a second hydrogen is donated and a water molecule and a diazene leave the ring leaving the deoxygenated product. In mechanism 2, hydrazine attacks a carbon in a meta position compared to the epoxide ring, and similar hydrogen donations occur to produce water and diazene leaving groups. This mechanism also results in a deoxygenated product. Reaction energy diagrams of these two mechanisms reacting with graphene sheets of increasing size suggest that reaction mechanism 1 is more dominant for larger aromatic sheets, but mechanism 2 is more common for smaller sheets[8].

Epoxide groups on the edge of a graphene oxide sheet were discovered to be more stable than those in the aromatic regions of the sheet[8]. For such epoxides, reaction mechanism

1 does not go to completion because the second step is has less free energy than the final step, and so a hydrozino alcohol product is the result of reacting hydrazine with edge epoxide groups. This reaction is a likely source of nitrogen in chemically modified graphene.

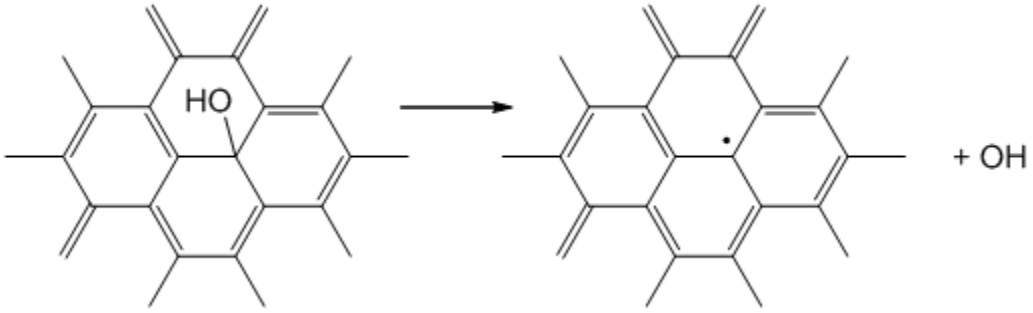

Figure 4. Spontaneous interior dehydroxylation of graphene oxide at room temperature

Additionally, Gao *et al*. suggests that reduction with hydrazine has little if any impact on the dehydroxylation of graphene oxide. According to their results, hydroxyl groups contained in the interior of an aromatic region of a graphene oxide sheet are thermodynamically unstable at room temperature and will spontaneously dissociate creating a graphene radical and a hydroxide radical as indicated in Figure 4.

In contrast, hydroxyl groups at the edge of a graphene sheet are stable at room temperature, and do not spontaneously dissociate and are not eradicated by hydrazine reduction. Increased temperatures exceeding 650˚C decrease the free energy barrier enough to remove edge hydroxyl groups from graphene oxide spontaneously, however edge epoxide groups remain.[8] Additionally, at temperatures exceeding 1000˚C carboxyl groups will spontaneously dissociate according to the mechanism proposed in Figure 5, as proposed by Gao *et al*.

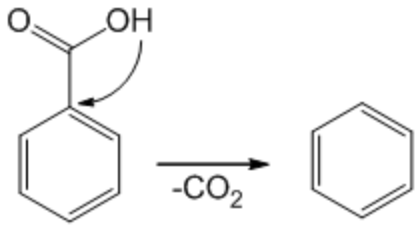

Figure 5. Mechanism for the spontaneous decarboxylation of graphene oxide at temperatures exceeding 1000 degrees Celcius[8]

A combination of both techniques for graphene oxide reduction would be desirable for the most thoroughly deoxygenated product because even when combined some oxygen impurities remain, but the combination of the two methods would remove the majority. The experiments considered in this paper used one reduction method or the other, not both which is one shortcoming of their experimentation.

Research conducted by Wang, Y. *et al.* focuses on modifying graphene intrinsically through n-type doping with nitrogen atoms. Chemical doping has proven to be a highly effective method for modifying the electrical properties of related materials such as carbon nano tubes[5]. Wang, Y. *et al*. produced nitrogen-doped graphene by exposing graphene coated electrodes to a nitrogen plasma atmosphere. The doped-graphene is further studied in their research to as an electrode material to explore the effect doping has on the electrical properties of graphene.

Wang D. *et al*. attempts to modify the chemical properties of graphene by introducing titanium oxide crystals into the lattice structure of graphene in the hopes of improving voltage capacity retention of the material under the stressful conditions of high charging and discharging rates. Their study tests the composite rutile and anatase TiO_2-graphene products as cathode materials in electrochemical cells. These cells are compared to cells using the pure metal oxide as the cathode material. Their results suggest that metal oxide-graphene compounds may provide a solution to resolve the issues with lithium ion insertion and extracton in lithium ion batteries.

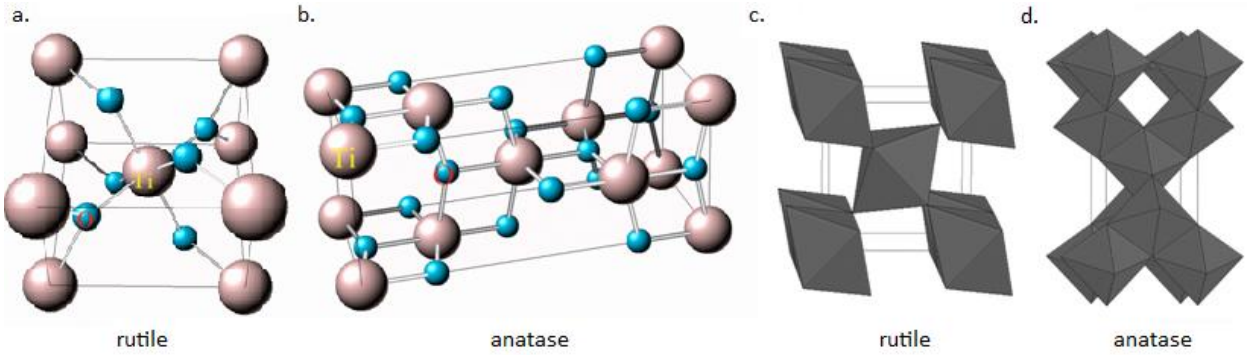

Figure 6. Structure of titanium dioxide presented as unite cells of rutile (a) and anatase (b) polymorphs as well as edge-sharing TiO_6 octahedral diagrams of rutile (c) and anatase (d) crystals

Rutile TiO_2 is the most common form with anatase and brookite as minor forms. Figure 6 displays the unite cell[9] and the octahedral diagrams[10,11] of TiO_6 for rutile and anatase titamium dioxide. Rutile TiO_2 has the lowest volume of the three most common forms and has a body-centered cubic unit cell. In the unit cell (6a) titanium ions have a co-ordination number of 6. This number means that 6 oxygen atoms surround the titanium ion in an octahedral pattern. Oxygen anions in the rutile form of TiO_2 have a co-ordination number of 3, which suggests that each oxygen atom is bound to 3 titanium ions. Anatase TiO_2 also has a rectangular unit cell (6b) but oxygen's in the lattice structure are bound differently. Oxygen in anatase TiO_2 also forms octahedral patterns around the titanium ion. Sometimes it is easier to visualize the crystal when drawn as edge-sharing TiO_6 octahedrons such as in Figure 6c and 6d. The anatase crystal structure is less dense than the rutile structure because the bond lengths are longer. Wang, D. et al. studies the effect on voltage capacity cells constructed with TiO_2-graphene composites using rutile and anatase crystals.

Wang, Y. *et al.* and Wang, D. *et al*. utilize some of the same techniques to analyze graphene in their respective work. Both used transmission electron microscopy (TEM) to obtain microscopic images of various reaction products. TEM is a form of microscopy that directs a

beam of electrons through a very thin sample to interact with the sample creating an image. This technique is very useful for creating images of surfaces, which is why both research groups utilized this technique in their work.

In addition to TEM, both groups used X-ray photoemission spectroscopy (XPS) to analyze the chemical state of different elements in bulk material. XPS analysis records the kinetic energy of core electrons emitted from atoms on the surface of a material using an electron spectrometer.[12] The core electrons are excited by photons of monochromatic light fired from an X-ray beam fired at the surface. The binding energy of a core electron to an atom is calculated from the measured kinetic energy of the ejected electron using the equation:

$$E_{binding} = E_{photon} - (E_{kinetic} + \emptyset)$$

where $E_{binding}$ is the binding energy of the electron, E_{photon} is the energy of the X-ray photons, $E_{kinetic}$ is the kinetic energy of the electron as measured by the electron spectrometer, and $\emptyset$ is the work done by the spectrometer.[12] Electron binding energies are unique to the atom and orbital they are emitted from[12]. This is partially due to the increasing positive charge of the nucleus as the atomic number increases. The more positive charge in the nucleus makes the binding energy of the $_{1s}$ energy level increase because the electrons become more and more attracted to the nucleus, which makes it more difficult to remove them. Unique binding energies make it possible to use XPS to study the state of different elements on a surface.

Cyclic voltammetry is another technique employed by Wang, Y. *et al*. to test the conductive properties of nitrogen-doped graphene. In cyclic voltammetry experiments, the

electric potential between a working electrode and a counter electrode is increased at a constant rate over time. This increase is called the scan rate. At a predetermined potential, the scan is switched and goes in reverse; decreasing over time. As the experiment progresses, any peaks that form outside the background wave of the scan correlate to the current of any analyte in solution. This peak can be either a reduction peak or an oxidation peak depending on the initial scan direction.[2] The crest (or trough if the peak is negative) of the peak indicates the reduction potential of the analyte. The peak degenerates as the analyte near the electrode is either reduced or oxidized, again depending on the direction. Wang, Y. et al. used this technique to study the application of nitrogen-doped graphene as an electrode material for electrochemical analysis.

These techniques help both research groups attain results specific to their experiments. Both experiments, though not necessarily related to each other, help to show that graphene is a highly conductive material that is easily modified to yield unique electrochemical properties with a wide variety of applications.

Results and Discussion

The goal of the Wang, Y. *et al.* was to develop a simple method for producing nitrogen-doped graphene sheets, and to investigate the capabilities of the hybridized material in electrocatalysis. Wang, Y. *et al.* produced nitrogen-doped graphene by exposing graphene sheets chemically synthesized using Hummers and Offemans[13] method and hydrazine reduction, to a nitrogen plasma atmosphere. Hummers and Offeman's method exposes graphite flakes to a mixture of sulfuric acid, sodium nitrate, and potassium permanganate to

make graphene oxide[13]. The graphite flakes are oxidized by the reaction with potassium permanganate, which is a strong oxidizing agent. The oxidation process separates the flakes into individual sheets of graphene oxide, which is the purpose of the oxidation. The graphene oxide produced was then reduced by hydrazine, N_2H_2.

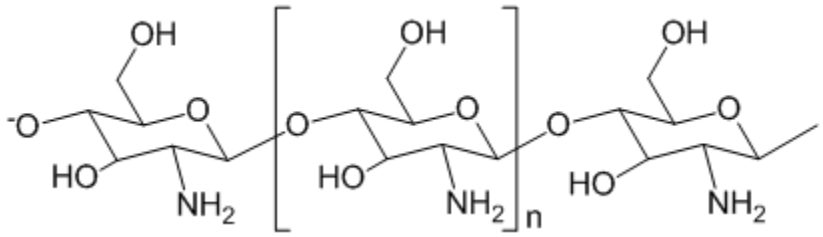

Figure 7. Chemical Structure of Chitosan

Wang, Y. *et al*. used the graphene to create a graphene-coated electrode in order to compare the electrocatalytic properties of graphene and nitrogen-doped graphene. To make the electrodes, synthetic graphene was mixed in chitosan (0.5 wt % with 2% acetic acid) with to form a 1 mg/ml graphene-chitosan solution.[5] Chitosan is a linear polysaccharide composed of repeating β-(1-4)-linked D-glucosamine and N-acetyl-D-glucosamine groups.[14] The structure of Chitosan is depicted in Figure 7. Commercial chitosan is derived chitin from the exoskeletons of crustacians.[14] Chitosan acts as a binding agent that allows the graphene sheets to adhere to the surface of a glassy carbon electrode because of the hydrophobic interface created between graphene and the glassy carbon.[5] Five micro liters of the graphene-chitosan mixture dried on the surface of a glassy carbon electrode to produce a graphene-coated glassy carbon electrode. Some of these electrodes are kept unaltered, and some are further modified to include nitrogen-doped graphene so comparisons can be made between the two materials.

To make the nitrogen-doped graphene electrodes, some of the graphene electrodes were placed in a plasma chamber that was filled with nitrogen gas pressurized to 750 mTorr[5]. The power of the plasma chamber was held at a constant 100 W, but the plasma treatment time varied incrementally from 20 to 100 minutes[5] in order to obtain a variety of nitrogen concentrations in the samples.

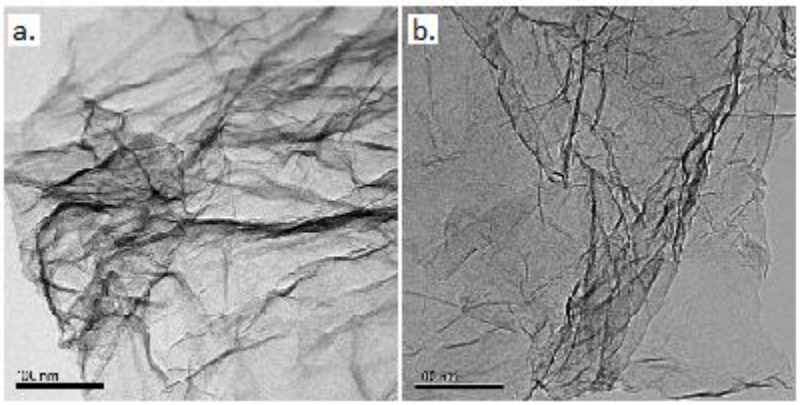

Figure 8. Transmission electron microscopy images of graphene (a) and nitrogen-doped graphene (b)

Figure 8 shows transmission electron microscope (TEM) images of chemically synthesized graphene in 8a, compared to nitrogen-doped graphene in 8b. The figure indicates that the two-dimensional geometry of the material remained after nitrogen-doping. Both images maintain the flat, sheet-like structure of graphene with its characteristic wrinkling and overlapping of sheets as indicated by the dark lines in the figures. Experimental analysis of the material was also conducted to confirm the integration of nitrogen into the graphene lattice.

Table 1 expresses the atomic percentage of oxygen, nitrogen and carbon in graphene and nitrogen-doped graphene in a comparative format. Two different areas were tested so one could examine whether the graphene sheets had a uniform composition. Uniform composition is supported by the data because the percentages of the different elements are very similar for

Table 1. Atomic Concentration of C, N and O in Synthetic Graphene and Nitrogen-Doped Graphene

Sample	Area	C_{1s} (%)	N_{1s} (%)	O_{1s} (%)
Graphene	1	84.26	0.18	15.56
	2	85.53	0.11	14.36
N-Doped Graphene	1	71.09	1.35	28.05
	2	72.77	1.26	26.54

Nitrogen-doped graphene was produced by exposing graphene to a nitrogen plasma treatment for 40 minutes at 750 mTorr of pressure and a power of 100 W. Two sample areas were tested for both graphene and nitrogen-doped graphene to help determine if even molecular distribution occurred.

both areas tested for the respective material. The values in Table 1 were obtained by XPS. The oxygen content of graphene and nitrogen-doped graphene is indicative of structural impurities not removed when graphene oxide was reduced. As mentioned earlier, Gao *et al*. determined that epoxide groups on the edges of the graphene sheets react via a different mechanism than those in the middle of the sheet. This alternative reaction mechanism is thermodynamically unfavorable after the second step, which results in the production of a hydrozino alcohol product.[8] In other words, epoxide groups at the edges of a graphene oxide sheet are converted to hydroxyl groups and add a hydrozino group to a ring reduced with hydrazine. With this understanding, it is sensible that the unaltered graphene would contain a small amount of nitrogen (0.145%) contributed by the reaction of edge epoxide groups with hydrazine. The atomic composition results in Table 1 also suggest successful nitrogen doping of the electrodes that were exposed to the nitrogen atmosphere because the nitrogen content of graphene rose to 1.35 percent.

In order to further confirm that the graphene sheets were successfully nitrogen doped, XPS of the graphene electrode was conducted. Comparative analysis of the XPS spectra for nitrogen-doped graphene and unaltered graphene yields dramatically different binding energy

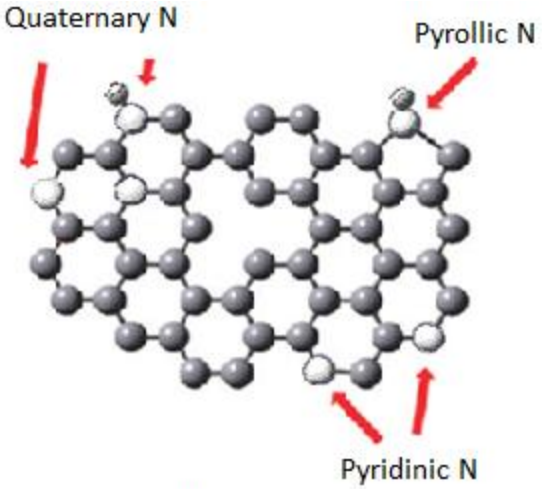

Scheme 1. A ball and stick model representing the lattice structure of nitrogen-doped graphene. Gray atoms represent carbon, while white atoms represent nitrogen and striped atoms represent hydrogen. A sample defect is displayed in the center of the diagram.

values (BE) for the N_{1s} binding energy range. The XPS spectra results are presented in Figure 9. The nitrogen peaks of the spectra for the nitrogen-doped graphene are present at BE = 398.9 eV for pyridinic nitrogen, N1; BE = 400.1 eV for pyrrolic nitrogen, N2; and BE = 401.5 eV for quaternary nitrogen, N3; as indicated in Figure 9b. This is in sharp contrast to the spectra results of pure graphene, which revealed no distinct peaks for nitrogen (9b). The large increase in peak height at the N_{1s} energy levels for nitrogen-doped graphene compared to graphene suggest that nitrogen was successfully integrated into the lattice structure of nitrogen-doped graphene. The results also reiterate that while nitrogen is largely absent from pure graphene, it is not non-existent. The important information relayed by this figure is the confirmation of the integration of nitrogen into the carbon lattice which is clearly evidenced by comparing the nitrogen peaks in Figure 9b to those of Figure 9a.

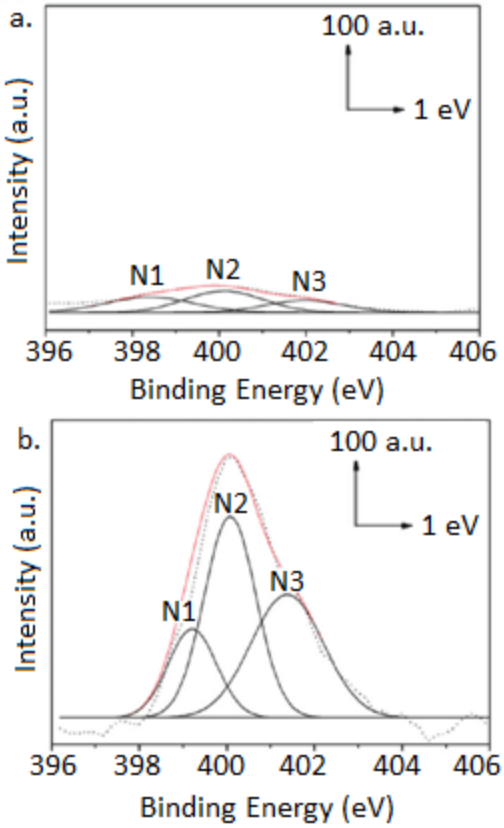

Figure 9. X-ray photoelectron spectra of graphene (a) and nitrogen-doped graphene (b) at N_{1s} binding energy range. N1 refers to pyridinic N, N2 refers to pyrollic N and N3 refers to quarternary N

The results of the XPS analysis (Figure 9) suggest that three types of N doping could have occurred. Scheme 1 depicts the structure of nitrogen-doped graphene and indicates the different ways nitrogen could be bound to the structure including pyridinic (N1), pyrrolic (N2) and quaternary (N3) integration of nitrogen into the structure.[5] Scheme 1 also shows a sample defect in the structure of graphene, as experimentation suggests these defects are very common.[8] Wang, Y. *et al.* did not study at length the effect different nitrogen binding types have on the conductive properties of graphene in this report, as it is not necessary to know how the nitrogen was bonded to the lattice in order to examine the general effect the binding has. However, pyrrolic nitrogen binding appears to be most prevalent according to the spectra seen in Figure 9b. Further studies should be conducted to determine if it is possible to selectively bind the nitrogen to graphene, and whether or not the different binding types impact the affect nitrogen has on graphene.

The nitrogen atoms that were embedded in the graphene sheet as a result of nitrogen doping introduce additional electrons into the lattice of the material because nitrogen has one more valance electron than carbon. These electrons enter a donor level of a molecular band model for graphene. The donor band decreases the band gap between the valence and conduction bands which increases electrical conductivity of the material because more electrons are able to reach the conductive band with less energy. This is the reason the electrochemical properties of the material are expected to increase upon the addition of such an impurity.

The successful doping of graphene is further evidenced by the XPS spectra taken from 282 to 290 eV, which is the C_{1s} binding energy range. These spectra are presented in Figure 10.

There are several different C groups in synthetic graphene, due to imperfections and impurities in the structure of the molecule[5]. It is likely that these impurities are derived from the incomplete reduction of graphene oxide because the impurities all contain oxygen. These imperfections cause several spectral peaks to form in the XPS spectra at the C_{1s} binding energy range, e.g. C-C at 284.8 eV, C1; C-OH at 285.9 eV, C2; C=O at 287.1 eV, C3; and O-C=O at 289.0 eV, C4; which can be seen in Figure 10a. When studying this result it is important to realize that the binding energy describing a C=O relationship is very close to that of a C-N relationship, which is approximately 287.5 ± 0.5 eV[5]. This fact is important because the two peaks overlap each other in the XPS spectrum.

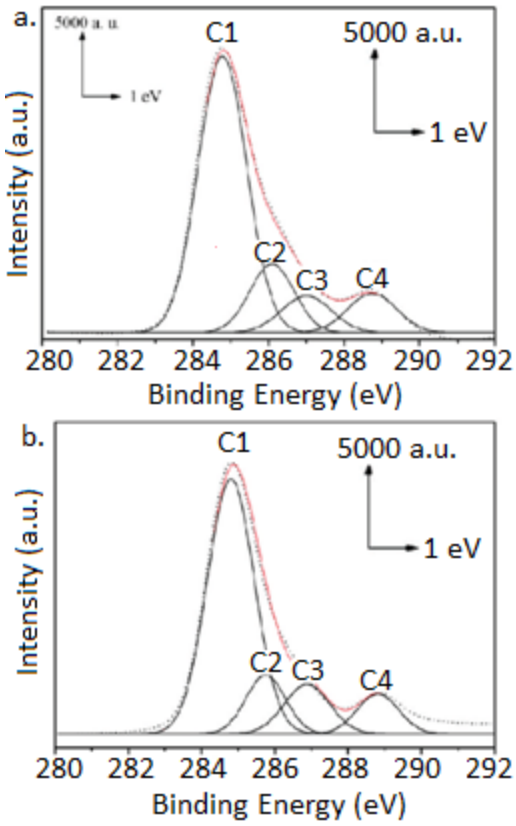

Figure 10. X-ray photoelectron spectra of graphene (a) and nitrogen-doped graphene at C_{1s} binding energy range. C1 refers to (C-C), C2 refers to (C-O), C3 refers to (C=O) and C4 refers to (O-C=O)

In order to confirm the presence of the C-N bonds, one must compare the spectra of the N-doped graphene (Figure 10b) to that of unaltered graphene, (Figure 10a) because both will contain C=O binding sites. Any increase in this peak for nitrogen-doped graphene over the corresponding peak in pure graphene must be attributed to C-N bonds, and thereby suggests successful nitrogen doping. As shown in Figure 10b, the peak at 287.1 eV for C=O/C-N is larger than the same peak in Figure 10a. This increase is due to the increased amount of nitrogen

present in the structure as a result of nitrogen doping. Overall, analysis of the XPS spectra obtained for nitrogen-doped graphene and unaltered graphene suggest that nitrogen was successfully integrated into the lattice structure of graphene in the nitrogen-doped samples. Nitrogen doping is expected to play an important role in improving the electrocatalytic activity of graphene.

While Wang, Y. *et al.* did not compare the effect different nitrogen binding types have on the conductive properties of graphene, they did obtain an optimum nitrogen plasma treatment time for the graphene electrodes. The optimum exposure time of the graphene electrodes to nitrogen atmosphere was determined by studying cyclic voltammetric measurements of 5 mM hydrogen peroxide with electrodes with exposure times of 20, 30, 40, 60 and 100 minutes. The results of these experiments are shown in Figure 11.

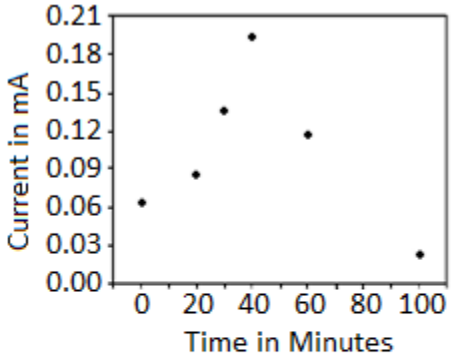

Figure 11. A plot of the cyclic voltammetric signal of 5 mM H_2O_2 versus plasma exposure time of the graphene coated glassy carbon electrode. Time 0 indicates no plasma treatment

The reduction current increased as the exposure time increased up to 40 minutes, but after that the current began to drop. It is possible that the longer exposure may tear or destroy the graphene layer on the glassy carbon electrode[5]. Based on the results in Figure 11, a 40 minute exposure time was determined to be the optimum time for producing nitrogen-doped graphene.

Nitrogen plasma exposure time was an important variable in the doping process because so many of the parameters were fixed. The volume of graphene solution for electrode

modification, the power of the nitrogen plasma, the chamber pressure, and the temperature were all constant throughout the nitrogen doping process[5]. Because all other variables remain constant, the amount of time the electrode was exposed to the nitrogen plasma is a determining factor for the amount of nitrogen that would bind to the material.

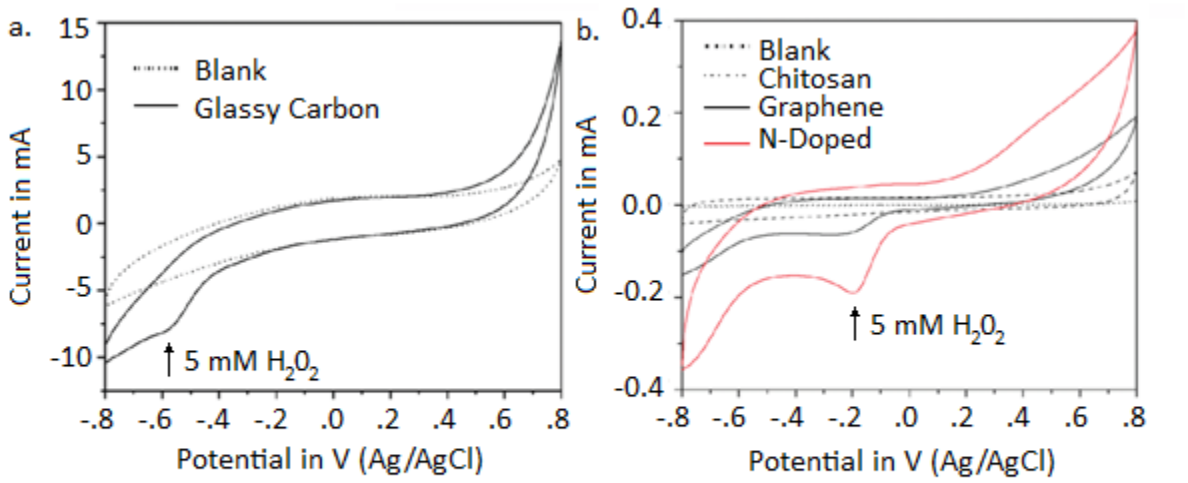

Figure 12. Cyclic voltammograms of a glassy carbon electrode in the presence and absence (Blank) of 5 mM hydrogen peroxide (a). Cyclic voltammograms of 5 mM hydrogen peroxide using a chitosan electrode, a graphene electrode and a nitrogen-doped graphene electrode (b)

The nitrogen-doped graphene electrode was used to study the electrochemical catalysis of 5 mM hydrogen peroxide using cyclic voltammetry. The cyclic voltammetry results obtained with the nitrogen-doped graphene electrode were compared with results obtained with an unaltered graphene electrode and a chitosan-coated electrode. The results of that experiment are depicted in Figure 12. The figure shows the responses of the different electrodes to hydrogen peroxide. The glassy carbon electrode showed a very weak response to 5 mM hydrogen peroxide, yielding an unresolved peak at -0.59 V of potential. Similarly, the graphene-coated glassy carbon electrode observed limited detection of the hydrogen peroxide; showing only a small peak at -0.21 V. The chitosan electrode showed indicated no detection of hydrogen peroxide at any voltage. In contrast, the nitrogen-doped graphene electrode

detected a reduction peak at -0.19 V which with a current of 200 μA. This peak is large and resolved, indicating an enhanced ability to detect hydrogen peroxide compared to both the glassy carbon electrode, and the unmodified graphene-coated glassy carbon electrode. The experiments conducted with the other electrodes indicate that the enhanced sensing capabilities are contributed by the effects of nitrogen doping, and not the addition of chitosan or graphene individually.

Wang, Y. *et al.* predicted that the high electron density and increased electrical conductivity[5] would facilitate nitrogen-doped graphene in reducing hydrogen peroxide. The benefit of using a nitrogen-doped graphene electrode compared to a glassy carbon electrode or even a pure graphene electrode for studying the electrical properties of hydrogen peroxide is that using nitrogen-doped graphene would make it easier to break the O-O bond in hydrogen peroxide because of the delocalized charges in the graphene[5].

These successful experiments of Wang, Y. *et al.* show that graphene has a promising future in electrochemistry due to its enhanced electro-catalytic activity when nitrogen doped. Their research may also be applicable to other carbon structures such as nanotubes and carbon fibers. Additional research on the different ways nitrogen bonds to the structure to determine if there is an optimal conformation within the lattice for nitrogen bonding and whether or not there is a way to selectively bond in one way could potentially improve the electrocatalitic activity of graphene even further.

The research conducted by Wang, D. *et al.* took a different approach to the modification of graphene. The goal of their research was to enhance the lithium ion insertion/extraction performance of TiO_2 crystals using graphene as a conductive molecular scaffolding from which

the materials could be assembled.[4] TiO_2 was selected as the metal-oxide in their experiments because it is a low-cost, abundant and environmentally benign material. Wang, D. et al. used TiO_2 in their experiments for this paper, but they acknowledge that other materials could have been used.

Wang, D. *et al.* used functionalized graphene prepared by the thermal expansion of graphene oxide. This differs from the hydrazine reduction method in that the graphene oxide undergoes rapid thermal expansion to separate it into functionalized graphene sheets and remove oxygen containing impurities. This method offers an alternative to chemical reduction for the production of graphene and many other materials. Unlike hydrazine reduction, thermal reduction removes edge hydroxyl and carboxyl groups from graphene oxide at high temperatures, but fails to remove the epoxide groups.[8] It is interesting that neither method used for graphene oxide reduction in these experiments is able to remove carbonyl groups.

To produce the metal oxide-graphene structures, Wang, D. *et al.* used a one-step process that would allow the self-assembly of the composite material. Graphene is hydrophobic molecule because the bonds in graphene are all carbon to carbon, which makes them non-polar. In contrast, the titanium oxide crystals are hydrophilic because of the di-pole moment created between the titanium atom and the electronegative oxygen atoms. The dipoles make the bonds in TiO_2 polar, which make the molecule hydrophilic. Naturally, hydrophilic molecules do not mix effectively with hydrophobic ones, so Wang, D. *et al.* used a surfactant molecule to bind the two together.

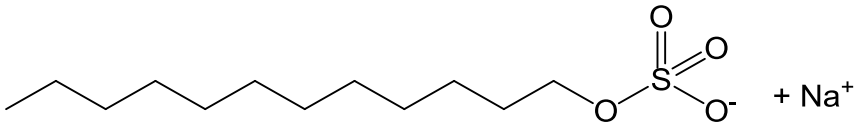

Figure 13. Chemical structure of sodium dodecyl sulfate; an anionic surfactant

A surfactant is a molecule with two different end groups that have an attraction to two different phases.[2] Surfactant molecules congregate in groups called micelles that form bilayers separating two phases. Wang, D. *et al*. used sodium dodecyl sulfate as the surfactant molecule in their experiments.

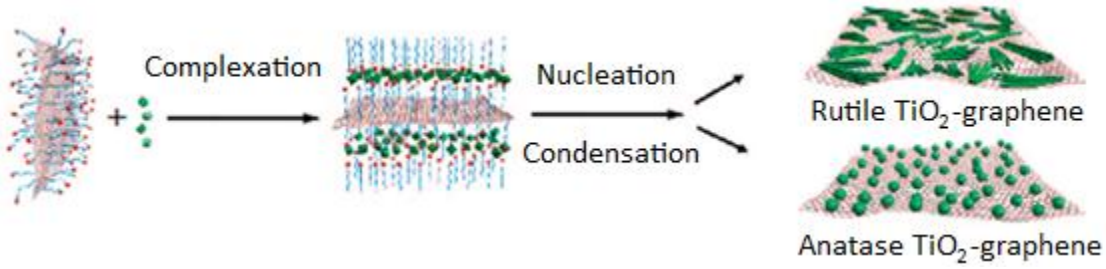

Scheme 2. Growth of rutile and anatase TiO_2-graphene composite materials as aided by anionic sulfate surfactant molecules. This Scheme was adapted from Wang, D. *et al*.

Scheme 2 illustrates this binding process. Production of the metal oxide-graphene complex is accomplished by adding the ionic sulfate surfactant to the graphene sheets and allowing in situ crystallization of the metal oxide to the graphene-surfactant skeleton. This process works because the surfactant molecule has both a hydrophobic and hydrophilic end, which can bind to both the graphene lattice and the metal-oxide components respectively.

When the anionic surfactant is added, it bonds to the graphene surface by its hydrophobic tail forming aqueous graphene-surfactant dispersion. The orientation of surfactant bonding leaves the hydrophilic sulfate head group exposed. The exposed sulfate groups are the ideal bonding site for the TiO_2 crystals because of the strong bond formed

between the two. This bonding results in the indirect adhesion of the crystals to the surface of graphene.

The materials underwent a low-temperature crystallization process in order to yield the desired rutile and anatase crystal formations, as well as to prevent the aggregation of the graphene layers. Rutile crystallization is the predominant result when $TiCl_3$ and H_2O_2 are added to the graphene-surfactant dispersion. To produce anatase crystals, $NaSO_4$ was added in addition to $TiCl_3$ and H_2O_2.

Figure 14a shows a TEM image of graphene sheets produced by rapid thermal expansion. This figure is similar to Figure 8, which shows graphene produced via chemical reduction with hydrazine (a) and nitrogen-doped graphene (b). Figures 8a, 8b, and 14a, all illustrate the planar geometry of graphene, as well as its slight tendency to wrinkle or adhere to other sheets. TEM images 14b and 14c show how the rod-like rutile TiO_2 crystals bind to the graphene surface. The difference in structure is evident when one compares figure 14a to figure 14b, wherein the dark rod-like regions illustrate rutile TiO_2 crystals which are lacking in figure 14a. Figure 14b offers a surface view of the material and illustrates that the rutile crystals lay in groups on the surface of graphene. Figure 14c is a cross-sectional TEM image that indicates

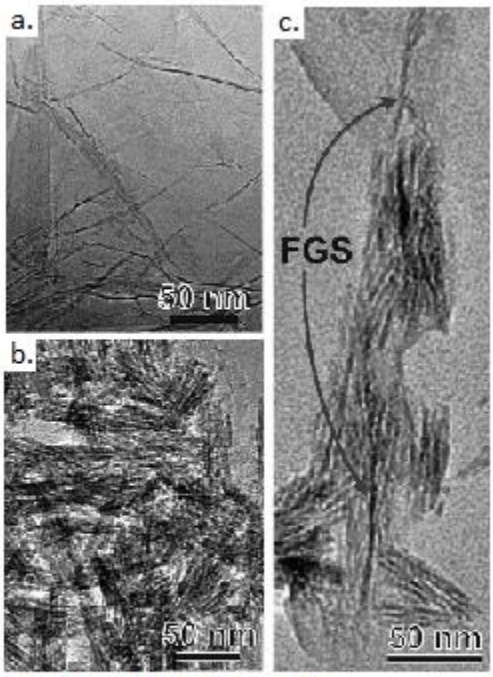

Figure 14. Transmission electron microscopy images of graphene (a) and rutile TiO_2-graphene composite structures in planar (b) and cross-sectional views (c)[3]

that the rutile TiO_2 crystals lie parallel to the surface of graphene, as opposed to jutting out perpendicular to the surface.

Figure 15 reveals the contrasting structure of anatase TiO_2-graphene in both plain field and dark field transmission electron microscopy images (Figure 15a and 15b respectively). These images show the more spherical crystal structure of anatase TiO_2, and show the even distribution of the crystals on the surface of the graphene sheet due to the use of surfactant molecules. Without this compound, few TiO_2-graphene bonds would form because of the repulsion between hydrophobic and hydrophilic molecules.

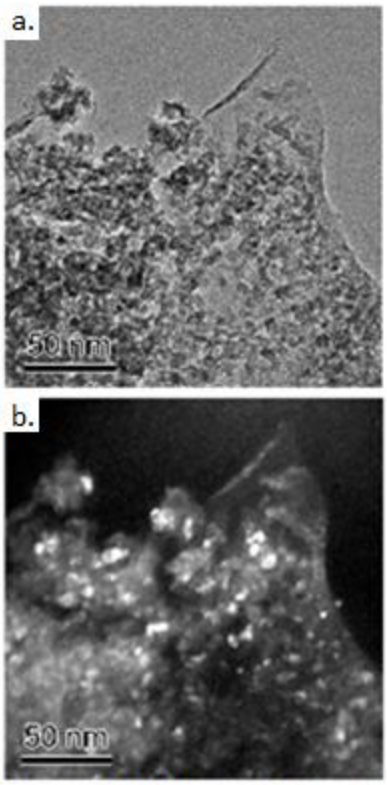

Figure 15. Plain-field (a) and dark-field (b) transmission electron microcopy images of anatase TiO_2-graphene[3]

The voltage capacities of electrochemical cells containing TiO_2 graphene composite materials were studied for comparison with the voltage capacities of electrochemical cells containing unaltered rutile and anatase TiO_2 crystals at different charge and discharge rates. The TiO_2-graphene composites were used as the cathode material in the experimental cells, while rutile and anatase TiO_2 crystals and conventional additives such as Super P® carbon, were used for the cathode in the respective control cells.

When analyzing these results it is important to realize that all batteries lose some capacity as the rate of charging or discharging increases because of internal energy losses due to resistance within the battery and the limited diffusion rate of ions through the electrolyte,

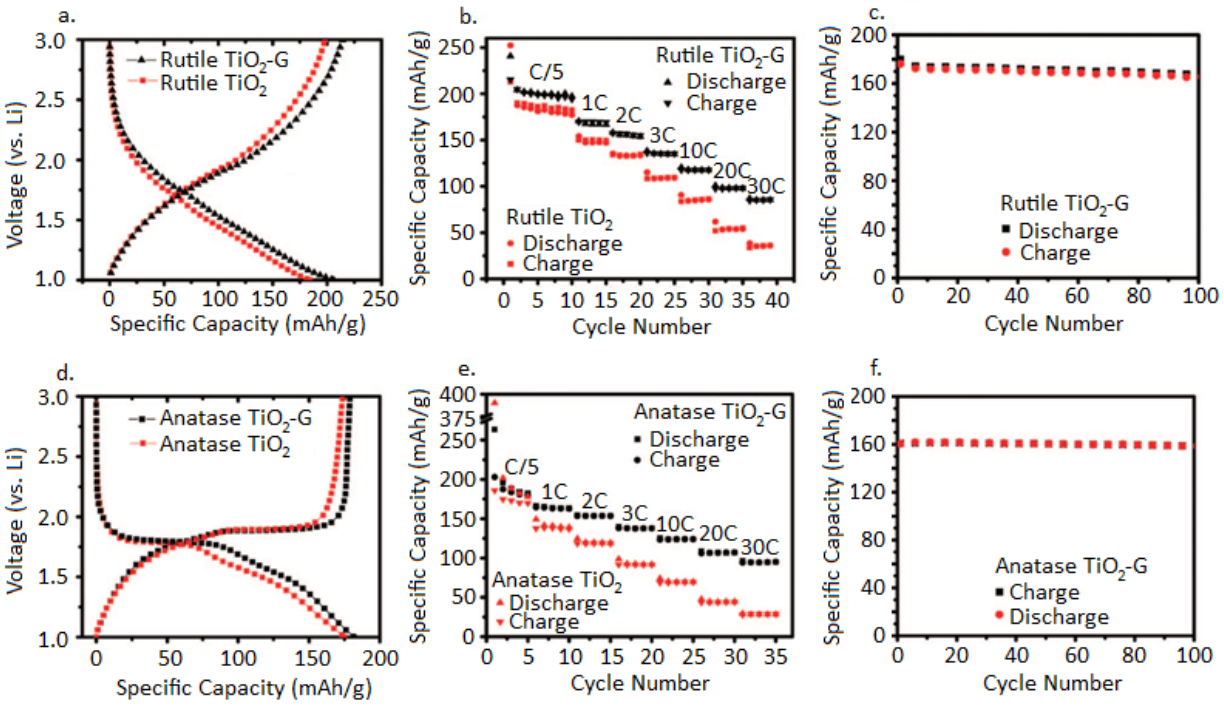

Figure 16. Charge and discharging profile of rutile TiO_2-graphene and rutile TiO_2 at 5 hour charge/discharge rates (a) Specific capacity of rutile TiO_2-graphene and rutile TiO_2 at difference charge/discharge rates (b) Specific capacity of rutile TiO_2-graphene over extended charge/discharge cycling (c) Charge and discharging profile of anatase TiO_2-graphene and anatase TiO_2 at 5 hour charge/discharge rates (d) Specific capacity of anatase TiO_2-graphene and anatase TiO_2 at difference charge/discharge rates (e) Specific capacity of anatase TiO_2-graphene over extended charge/discharge cycling (f)

which can only move so quickly.[15] Additionally, in the specific capacity vs. cycle number graphs, 1C refers to the amount of current required to charge the battery in one hour's time.[15] By that logic, a charge rate of 30C delivers the amount of current required to charge the battery in two minutes. A discharge rate of 30C has the opposite effect; the electrical energy stored in the battery is delivered at a current such that the battery "dies" after two minutes. The different rates of charge and discharge contribute to the loss of voltage capacity sustained by the cell, but different materials are affected by high charge/discharge rates differently, as the results suggest is the case with the TiO_2-graphene modified materials.

The rutile TiO_2-graphene electrode had a voltage capacity profile that mimicked the profile of a control rutile TiO_2 at a charge/discharge rate of C/5 or 5 hours as can be seen in Figure 16a. This result suggests that the structure of the crystals has not been altered; they have just been bound to the graphene surface via the surfactant micelles, because the charge and discharge profiles of the materials do not differ significantly. Figure 16b illustrates that for the rutile TiO_2-graphene material, the specific (i.e. voltage) capacity decreased for all charge and discharge rates, as did the control rutile TiO_2 crystals. However, the decrease in voltage capacity of the rutile TiO_2-graphene containing cells occurred at a slower rate than that of the rutile TiO_2 cells. In Figure 16c, the almost horizontal line indicates that at a 1C rate, the specific capacity of rutile TiO_2-graphene containing cells is consistent for at least 100 cycles, which means the battery can be drained and recharged at least a hundred times without losing capacity; correlating to the longevity of the battery.

Similarly, the voltage capacity of the anatase TiO_2-graphene product shows results resembling the control anatase TiO_2. Again, this is indicative of maintained crystal structure after binding to surfactant molecules. The voltage capacity relationships between anatase TiO_2 and the anatase TiO_2-graphene material are depicted in Figure 16d. The specific capacity of the anatase TiO_2-graphene also decreased at all charge/discharge rates which can be seen in Figure 16e. Once again the relative decrease in voltage capacity was less for the anatase TiO_2-graphene containing cell, compared to the more dramatic decrease in voltage capacity of the anatase TiO_2 containing cell as charge and discharge rates increased. Additionally, in Figure 16f the horizontal line indicates that at a 1C rate, the specific capacity of the anatase TiO_2-graphene containing cells was consistent for 100 cycles; again correlating to the longevity of the battery.

These results indicate that while both crystal forms of the graphene-modified materials lose their ability to hold charge as the rate of charging and discharging increases, the TiO_2-graphene composite electrodes were better able to maintain charge carrying capabilities compared to the cells containing electrodes with the respective TiO_2 crystals alone. Interestingly, the specific capacity of anatase TiO_2-graphene illustrated in 16f appears to be more consistent over time than its rutile counterpart in 16c which may indicate that the anatase form is more stable as an electrode material, although the difference indicated by the figures is admittedly minute.

Wang, D. *et al*. conducted impedance spectroscopy analysis of the rutile TiO_2-graphene materials in order to study why the graphene modified materials are better able to maintain voltage capacity. They discovered that the resistivity within the cells decreased from 93Ω using pure rutile TiO_2 to 73Ω when 0.5% by weight graphene was added to the electrode[4] (as the composite TiO_2-graphene material). This decrease in resistance of the cells indicates that improved ability to maintain voltage capacity in the modified materials may be contributed by the increased conductivity of the crystals due to their bond with graphene.

Conclusion

The experiments conducted by Wang, Y. et al. and Wang, D. et al. describe the variety of electrical capabilities of graphene. Through nitrogen-doping, graphene can be used in electrochemical sensing as an electrode material. Wang, Y. et al. showed this to be true through the use of nitrogen-doped graphene electrodes to sense 5 mM hydrogen peroxide in cyclic voltammetry experiments where the nitrogen-doped graphene electrode showed enhanced electrochemical sensing abilities of hydrogen peroxide compared to glassy carbon

electrodes as well as unaltered graphene electrodes. Furthermore, the use of graphene as a cathode material in lithium ion batteries as studied by Wang, D. et al. proved to be a very promising endeavor. The increased voltage capacity of electrochemical cells that used TiO_2-graphene composite materials had improved voltage capacity retention as charge and discharge rates increased compared to TiO_2 alone. This result likely occurs because of increased conductivity due to the addition of graphene, which was shown to reduce internal resistance of the cell by Wang, D. et al. These two very different experiments that both use graphene to modify electrochemical properties of different additives gives one a glimpse of the potential graphene has as a nano-material. Graphene is a nano-material that the scientific community has only just begun to understand, but so far it is already proving to be a highly adaptable and effective material for electrochemical applications.

References

(1) Brain, M. HowStuffWorks "How Lithium-ion Batteries Work".
(2) Harris, D. *Quantitative chemical analysis*; 7th ed.; W.H. Freeman and Co.: New York NY, 2007.
(3) Brain, M. HowStuffWorks "How Electric Cars Work".
(4) Wang, D., D.; Choi, D.; Li, J.; Yang, Z.; Nie, Z.; Kou, R.; Hu, D.; Wang, C.; Saraf, L. V.; Zhang, J.; Aksay, I. A.; Liu, J. *ACS Nano* **2009**, *3*, 907-914.
(5) Wang, Y., Y.; Shao, Y.; Matson, D. W.; Li, J.; Lin, Y. *ACS Nano* **2010**, *4*, 1790-1798.
(6) Kim, H.; Abdala, A. A.; Macosko, C. W. *Macromolecules* **2010**, *43*, 6515-6530.
(7) Rao, C. N. R.; Sood, A. K.; Voggu, R.; Subrahmanyam, K. S. *J. Phys. Chem. Lett.* **2010**, *1*, 572-580.
(8) Gao, X.; Jang, J.; Nagase, S. *J. Phys. Chem. C* **2010**, *114*, 832-842.
(9) The Saiful Islam Research Group - Research Themes.
(10) Kinsinger, N. M.; Wong, A.; Li, D.; Villalobos, F.; Kisailus, D. *Crystal Growth & Design* **2010**, 101020082930057.
(11) Reyes-Coronado, D.; Rodríguez-Gattorno, G.; Espinosa-Pesqueira, M. E.; Cab, C.; de Coss, R.; Oskam, G. *Nanotechnology* **2008**, *19*, 145605.
(12) Skoog, D. *Principles of Instrumental Analysis.*; 6th ed.; Thomson Brooks/Cole: Belmont CA, 2007.
(13) Hummers, W. S.; Offeman, R. E. *J. Am. Chem. Soc.* **1958**, *80*, 1339-1339.
(14) Pavinatto, F. J.; Caseli, L.; Oliveira, O. N. *Biomacromolecules* **2010**, *11*, 1897-1908.
(15) Buchmann, I. Discharge Methods.